Biosensors and Bioelectronics 25 (2010) 2458–2463

Contents lists available at ScienceDirect

Biosensors and Bioelectronics

journal homepage: www.elsevier.com/locate/bios

Direct growth of nanoporous Au and its application in electrochemical biosensing

A.K.M. Kafi [a], Asieh Ahmadalinezhad [a], Jingpeng Wang [a,b], Dan F. Thomas [b], Aicheng Chen [a,*]

[a] Department of Chemistry, Lakehead University, Thunder Bay, Ontario P7B 5E1, Canada
[b] Department of Chemistry, University of Guelph, Guelph, Ontario N1G 2W1, Canada

ARTICLE INFO

Article history:
Received 21 March 2010
Received in revised form 2 April 2010
Accepted 6 April 2010
Available online 13 April 2010

Keywords:
Nanoporous Au
Hemoglobin
Biosensors
Hydrogen peroxide

ABSTRACT

In this work, we have directly grown three-dimensional nanoporous Au networks onto a Ti substrate using the hydrothermal technique. This newly designed material with a large surface area was used as a supporting matrix for immobilizing a redox protein, hemoglobin (Hb), to develop a high-performance hydrogen peroxide biosensor. Scanning electron microscope (SEM), X-ray photoelectron spectroscopy (XPS), and energy-dispersive X-ray (EDX) spectroscopy were employed to characterize the morphology and composition of the fabricated nanoporous Au network. Cyclic voltammetry (CV) and amperometry were used to study and to optimize the performance of the fabricated electrochemical biosensor. Our CV studies show the direct electron transfer of Hb immobilized on the nanoporous Au network. In addition, amperometric H_2O_2 sensing experiments revealed that the nanoporous Au-network based biosensor exhibits fast response, long linearity, a low detection limit, high stability and very good reproducibility. Under the optimized conditions, the linearity of the developed biosensor for the detection of H_2O_2 spans from 5×10^{-8} to 2×10^{-4} M with a detection limit of 2×10^{-8} M (based on S/N = 3).

1. Introduction

The focus of this work is to synthesis nanoporous Au material and to explore its promising applications in electrochemical biosensor design. Research and development in the biosensor field is wide and multidisciplinary, found in biochemistry, physical chemistry, electrochemistry, electronics, biotechnology, nanotechnology and software engineering (Batchelor-McAuley et al., 2009; Kissinger, 2005; Wanekaya et al., 2008; Luong et al., 2008; Kafi and Chen, 2009). Biosensors have a wide range of applications in the domains of clinical diagnostics, environmental monitoring, forensic chemistry, pharmaceutical studies, food quality control, and biological warfare detection (Wang, 2008; Yang et al., 2009). A variety of transducer technology has been employed for the development of biosensors. One of the common approaches is the electrochemical method due to its high sensitivity, simplicity and cost competitiveness (Mehrvar and Abdi, 2004; Benvenuto et al., 2009). The big challenge in creating biosensors is to find and develop proper conjugation strategies between electrodes and biological molecules such as enzymes (Liu et al., 2006; Tian et al., 2007). It is desirable to detect a large number of chemical and biochemical substances in a direct way and with low detection limits. Thus, there is great interest in improving the transducer technology to allow direct detection and to increase the number of analytes that can be measured using the biosensor technology. In this context, progress in nanotechnology allows the development of highly sensitive biosensors with the additional advantage of miniaturization (Gooding, 2006). Nanostructured materials have been identified as desirable immobilization matrices due to their high active surface areas for enzyme binding, regular structures, and good mechanical, thermal and chemical stability (Wang et al., 2003; Katz and Willner, 2004; Liu and Chen, 2005; Kafi et al., 2008; Highton et al., 2009). Nanostructured materials are expected to possess much higher surface areas and have attracted great attention in a wide range of electrochemical applications (Michel et al., 2007; Koczkur et al., 2007; Huang and Sun, 2005). Nanostructured gold is an emerging material for use in various applications, notably in fuel cells, sensors, biosensors, DNA sensors, and bioanalytical diagnostics platforms (Beissenhirtz et al., 2007; Matthew et al., 2007; Zeis et al., 2007; Kongcheng et al., 2008; Shulga et al., 2008; Lim et al., 2008).

Sensitive detection of H_2O_2 is of central importance in environmental, pharmaceutical, biomedical research, and industrial settings (Wang and Wang, 2004; Chen and Dong, 2007). Several electrochemical biosensors based on redox enzymatic activity such as horseradish peroxidase (HRP) or enzymatic-like activity such as hemoglobin (Hb) have recently been designed for H_2O_2 detection (Duan et al., 2008; Feng et al., 2005; Kafi et al., 2008; Zheng et al., 2008a,b; Zhu et al., 2009). It is well known that the structural properties inherent in the enzymes/proteins such as HRP or Hb make it difficult to achieve direct electron transfer when they are directly immobilized on conventional electrode surfaces such as glassy carbon, gold and platinum (Yan et al., 2005). The per-

* Corresponding author. Tel.: +1 807 3438318; fax: +1 807 3467775.
E-mail address: aicheng.chen@lakeheadu.ca (A. Chen).

0956-5663/$ – see front matter © 2010 Elsevier B.V. All rights reserved.
doi:10.1016/j.bios.2010.04.006

formance of a biosensor mainly depends on the properties of the bioactive layer associated with the transducer. However, it is often still the case that the redox enzymes/proteins are too large to interact directly with a conventional electrode without being at least partly denaturated of biomaterials. Since the active sites of these enzymes/proteins are deeply buried in protective protein matrixes, an exceptional working condition is required in order to achieve direct electron exchange with the electrode. In this context, inorganic nanotubes, nanoparticles (NPs) and colloids are attracting growing attention owing to their specific characteristics of large specific surface area for enzyme adsorption and good biocompatibility (Katz and Willner, 2004; Ahmadalinezhad et al., 2009). Nanoporous gold (NPG) is a new kind of nanomaterial with prominent properties which make it an attractive material in biosensor development. It is expected that nanoporous gold can be a good carrier for biomacromolecules due to its pore structure, large surface area and high-specific pore volume. To the best of our knowledge, there is no existing efficient method to directly grow nanoporous Au except a few reports on the synthesis of nanoporous Au by chemical/electrochemical dealloying from binary or multicomponent Au-based alloys (Erlebacher et al., 2001; Zhang et al., 2007; Xu et al., 2007).

HRP is the most commonly used enzyme for the fabrication of H_2O_2 electrochemical biosensors. Owing to its expensiveness and unstableness, finding alternatives to reduce the cost and to improve the performance of H_2O_2 biosensors is scientifically interesting and important practically. Although Hb does not function as an enzyme in biological systems, it is an inexpensive model system for HRP and its peroxidase activity is well documented (Kumar and Chaudhari, 2002; Li et al., 2006). In this study, for the first time, we have immobilized hemoglobin (Hb) on nanoporous Au networks directly grown on Ti substrates by the chemical reduction of an Au precursor under a hydrothermal condition. Our electrochemical study reveals that the immobilized Hb exhibits direct electrochemistry and high catalytic activity toward hydrogen peroxide. The fabricated Au-network based biosensor exhibits fast response, long linearity, a low detection limit, high stability and very good reproducibility for H_2O_2 detection.

2. Experimental

2.1. Reagents and materials

Hemoglobin was purchased from Sigma and used as received. Stock solutions were stored at a temperature of 4 °C. The chitosan was from Aldrich. 30% hydrogen peroxide was bought from Fluka and the stock solutions of H_2O_2 were diluted from this. The experimental solutions were prepared every day by appropriate dilution of the stock solution. All other reagents were of analytical grade and were used as supplied. Water was purified with the nanopure water system and was used to prepare all solutions. All experiments were performed in 0.1 M phosphate buffer solution (PBS), maintaining different pH values with K_2HPO_4 and KH_2PO_4.

2.2. Biosensor fabrication

The nanoporous Au networks used in this study were synthesized by chemical reduction of an Au precursor under a hydrothermal condition (Holt-Hindle et al., 2008; Wang et al., 2008). Briefly, a Ti plate (99.2% from Alfa Aesar, cut into small pieces, 1.25 cm × 0.80 cm, with a thickness of 0.5 mm) was washed in acetone followed by nanopure water, and then etched in an 18 wt% HCl solution at 85 °C for 10 min. The etched Ti substrate was transferred into a Teflon lined autoclave containing 4.2 mM $HAuCl_4$ and 0.36 wt% formaldehyde. Then the autoclave was sealed and heated at 180 °C for 8 h. After cooling to room temperature, the Au-coated Ti plate was annealed in a tube furnace at 250 °C under argon protection for 2 h and then rinsed with pure water. Finally, 20 μL of 2 mg/ml of HB was co-immobilized onto the nonporous Au-network modified Ti electrode with 10 μL of 2 mg/ml of chitosan. The resulting electrode is referred to as Ti/NP–Au/Hb. Chitosan has been used for fabricating highly stable biosensors and is used here to enhance the stability of the biosensor (Khan and Dhayal, 2008). For comparison, two other kinds of electrodes, Ti/Hb and Ti/Au/Hb, were fabricated using a Ti plate and a Ti substrate modified by a sputtered Au thin film, respectively. The Au thin film was coated onto a Ti substrate by argon plasma sputtering for 30 s. The modified electrodes were stored in a phosphate buffer solution with a pH of 7.0 at 4 °C when not in use.

2.3. Instrument and electrochemical measurements

The morphology and the composition of the synthesized nanoporous Au network was characterized by scanning electron microscope (SEM) (JEOL JSM 5900 LV) at an acceleration voltage of 13 kV, X-ray photoelectron spectroscopy (XPS), and an energy-dispersive X-ray (EDX) spectrometer. Electrochemical measurements were carried out with a CHI (630B) workstation. A three-electrode configuration was employed for these experiments. The modified nanoporous Au-network–Ti electrodes were employed as the working electrodes. A platinum coil was employed as the counter electrode and a 3 M KCl saturated Ag/AgCl electrode was connected as the reference electrode. Cyclic voltammetric measurements were carried out in 0.1 M PBS by scanning the electrode potential in the range between 0.1 and −0.5 V versus Ag/AgCl. Amperometric responses were measured in 0.1 M PBS stirred by a magnetic stirrer. All measurements were performed at room temperature. Prior to the experiment, all electrolytes were deoxygenated by bubbling ultra-pure argon for 20 min and an argon atmosphere was maintained during the course of the experiments.

3. Results and discussion

3.1. SEM, XRD and XPS studies of the nanoporous Au-network modified Ti

The nanostructures of the fabricated nanoporous Au networks onto the Ti electrodes was examined by SEM. Fig. 1 shows typical SEM images of the nanoporous Au networks fabricated in this study at 3000× and 15,000× magnifications. The low magnification SEM image (Fig. 1a) shows that the Ti substrate is well covered by abundant gold nanoparticles and chain-like fibers. The high magnification SEM image (Fig. 1b) reveals that the nanoparticles and chain-like fibers are interconnected, forming three-dimensional networks. The diameter of the formed randomly porous structures varies from tens to hundreds of nanometers. Fig. 1c displays the EDS of the synthesized Au networks. Strong Au peaks appear in the EDS spectrum; but no discernible carbon or oxygen signals are observed, showing that the synthesized Au-nanoporous networks are free of organic impurities. Fig. 1d presents the XRD patterns of the nanoporous Au network. All the peaks labelled by an asterisk are derived from the Ti substrate. The lattice constant calculated from the pattern was 4.079 Å, consistent with the literature a = 4.078 Å (Joint Committee on Powder Diffraction Standards file no. 04-0784). The average crystallite size was calculated to be 22 nm, indicating that the discernible particles in the SEM images are actually agglomerated crystallites. We further characterized the nanoporous Au network using XPS. Fig. 1e displays the XPS spectrum of the Au 4f region. The dots, dotted line, red and blue solid lines, and black solid line represent the raw data, base

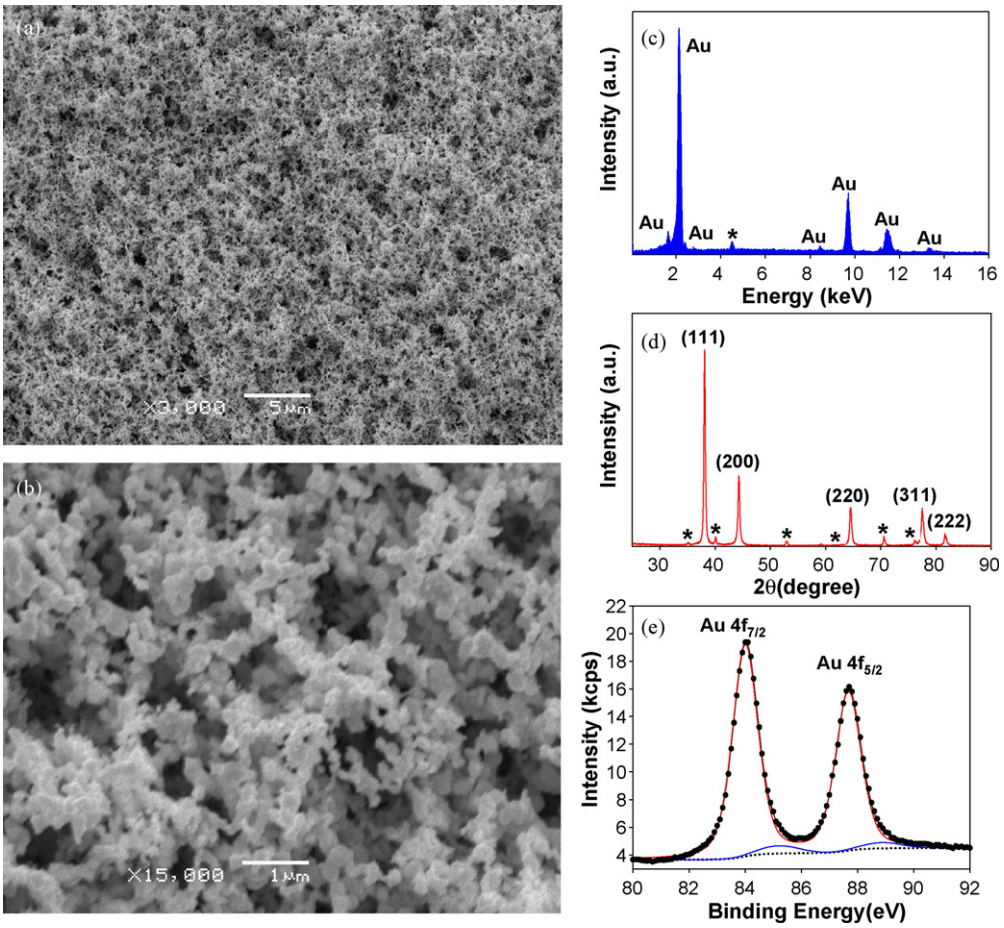

Fig. 1. (a and b) SEM images of nanoporous Au networks recorded at various magnifications. (c) EDS spectrum of the synthesized nanoporous Au networks; peak labelled by an asterisk is attributed to the Ti substrate. (d) XRD spectrum recorded from the synthesized nanoporous Au network. (e) XPS spectra of the Au 4f region for the as-synthesized nanoporous Au network.

line, individual components and total fit, respectively. The two 4f binding states of zero valences Au are identified as $4f_{7/2}$ and $4f_{5/2}$ at 84.0 and 87.7 eV, respectively, which are highly consistent with the literature (Moulder et al., 1995). Results from the spectral area integration of individual components indicate that 95.4% of the Au exists as zero valence species, whereas the other 4.6% represents species in oxidation states. This high percentage of metallic species suggests a highly effective reduction of the gold precursor through the applied hydrothermal process.

3.2. Direct electrochemistry of Hb immobilized onto the nanoporous Au network

The direct electrochemistry of Hb immobilized onto the nanoporous Au network was investigated using cyclic voltammetry. Fig. 2a displays the CVs of the Ti/NP–Au/Hb (dashed line) and the Ti/NP–Au electrode (solid line) recorded in the potential range from −0.5 to 0.1 V at a scan rate of 20 mV/s in 0.1 M PBS (pH 7.0). As expected, the CV of the Ti/NP–Au electrode is featureless. In contrast, the Ti/NP–Au/Hb electrode shows a couple of well-defined peaks, the oxidation peak at −0.125 V and reduction peak at −0.21 V. The formal potential E_0 of Hb was thus calculated to be −0.167 V, which is more negative than the redox potential of native Hb (−0.048 V). This is likely due to the interactions between the immobilized Hb and the nanostructured surface, leading to a structural alternation from the closed structure in the native state of Hb to an open conformation and thereby resulting in a decrease in the redox potential (Yan et al., 2005). Normally redox proteins/enzymes do not show any electroactivity at conventional bare electrodes under the same conditions (Gao and Gao, 2007), and no redox peaks are seen in the CVs of the Ti/Hb and Ti/Au/Hb electrode (data not shown). The above results reveal that the redox peaks are attributed to the direct electron transfer of the immobilized Hb onto the nanoporous Au network and that the nanoporous Au network plays an important role in the enhancement of the electroactivity of the immobilized Hb.

Fig. 2b shows the CVs of the Ti/NP–Au/Hb electrode recorded in 0.1 M pH 7.0 PBS at different scan rates. A pair of nearly symmetric anodic and cathodic peaks appears with almost equal peak currents when the scan rates were varied from 5 to 100 mV/s. This is due to the fact that the electroactive Hb Fe (III) immobilized on the nanoporous Au is reduced to Hb Fe (II) on the forward scan and then reoxidized to Hb Fe (III) during the reverse scan. In addition, the peak-to-peak separation increases with the increase of the scan rate. As seen in Fig. 2c, the anodic peak current and the cathodic peak current linearly increase with the increasing of the scan rate, showing that the redox process of the immobilized Hb is quasi-reversible and surface controlled (Murray, 1984).

3.3. Catalytic activity to H_2O_2 reduction

Electrocatalytic reduction of H_2O_2 on the Ti/NP–Au/Hb electrode was further examined. Fig. 3 shows the voltammograms of the Ti/NP–Au/Hb electrode recorded in 0.1 M pH 7.0 PBS in the presence (ii and iii) and the absence of H_2O_2 (i). Comparison of Plot i (dotted line) and Plot ii (dashed line) shows that after the addition of

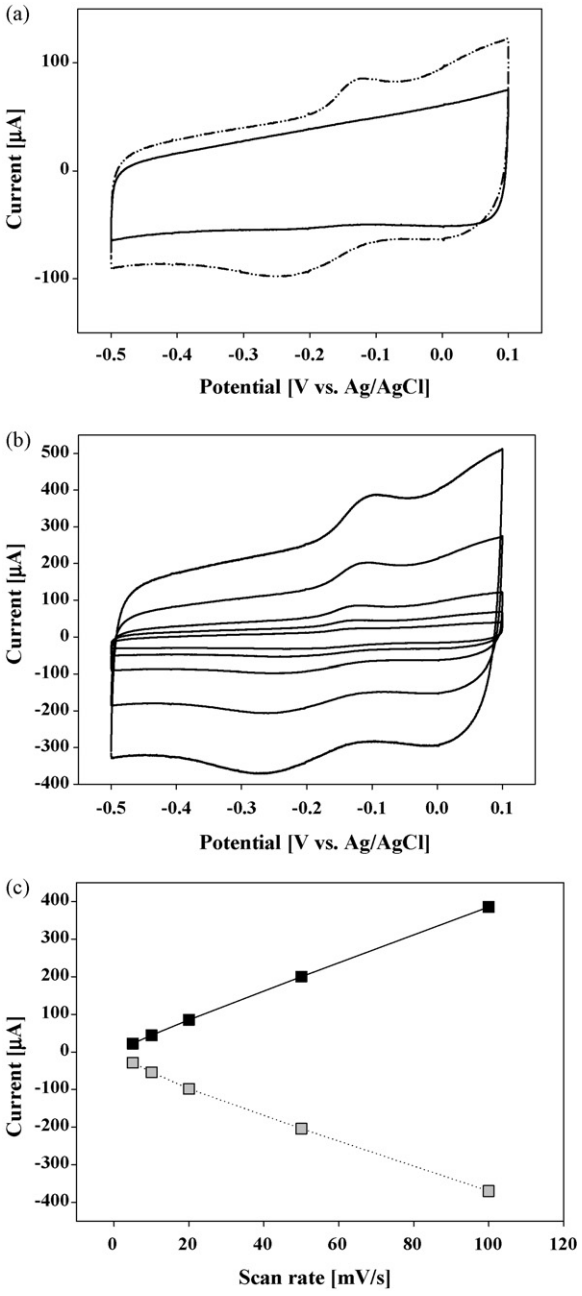

Fig. 2. (a) Cyclic voltammograms of the Ti/NP–Au/Hb (dashed) and the Ti/NP–Au electrode (solid) in 0.1 M PBS with pH 7.0 at a scan rate of 20 mV/s. (b) Cyclic voltammograms of the Ti/NP–Au/Hb electrode with different scan rates in 0.1 M PBS with pH 7.0. The scan rates were from 5 to 100 mV/s. (c) Oxidation and reduction current versus scan rates.

0.25 mM H_2O_2, the reduction peak current increases accompanied by a decrease of the oxidation peak current. However, no noticeable response was found at the Ti electrode and very low response to H_2O_2 was found for the Ti/Hb electrode (data not shown here), showing that the catalytic reduction of H_2O_2 indeed originates from the Hb immobilized on the nanoporous Au network. The reduction current increases with the increment of the H_2O_2 concentration from 0.25 (ii) to 0.5 mM (iii). The above results indicate that the immobilized Hb in the Au films retained its bioactivity on the electrode surface and show excellent electrocatalytic activity for the reduction of H_2O_2. The generic reaction for reduction of H_2O_2 by Hb can be expressed as the following (Wang et al., 2009):

$$Hb(Fe^{3+}) + H_2O_2 \rightarrow \text{CompoundI}(Fe^{4+}{=}O) + H_2O \quad (1)$$

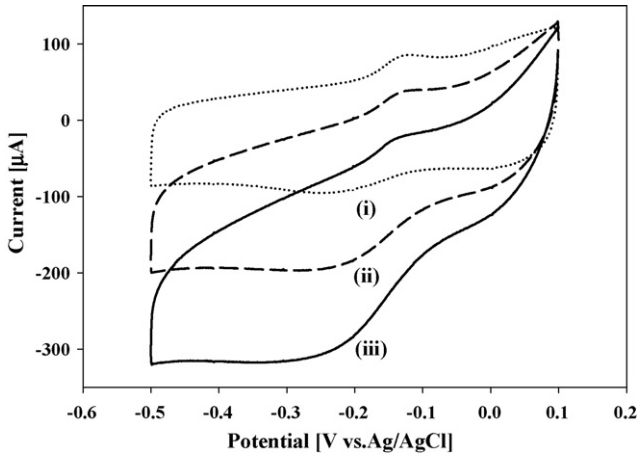

Fig. 3. Cyclic voltammograms of the Ti/NP–Au/Hb electrode (i) in the absence of H_2O_2 and in the presence of 2.5×10^{-4} M (ii) and 5×10^{-4} M (iii) H_2O_2 in PBS with pH 7.0 at the scan rate of 20 mV/s.

$$\text{CompoundI}(Fe^{4+}{=}O) + 2e + 2H^+ \rightarrow Hb(Fe^{3+}) + H_2O \quad (2)$$

Given the above reaction, the added H_2O_2 increases the oxidation form of the heme group in the proximity of the electrode, resulting in increased cathodic current and the disappearance of the anodic current.

3.4. Optimal conditions for working with the biosensor

Working under suitable applied potential is very important for biosensors in order to obtain maximum response. Thus the effect of applied potential on the response of the Ti/NP–Au/Hb electrode to H_2O_2 was examined. As shown in Fig. 4a, when the applied electrode potential was decreased from +0.1 to 0.0 V, the reduction current slightly increased; then dramatically increased when the electrode potential was decreased from 0.0 to −0.3 V; further decreasing the electrode potential, the reduction current slightly decreased. At more negative potentials there is a chance of interference reactions from other electroactive species in the solution. The electrode potential −0.3 V was thus selected as the optimized potential after an overall consideration of the detection sensitivity, where the background current is minimized and unexpected interfering reactions of other electroactive species can be avoided effectively.

The pH value of the buffer solution is another key factor that could affect the behavior of the H_2O_2 biosensor. Fig. 4b shows the steady-state reduction current response of the Ti/NP–Au/Hb biosensor to H_2O_2 at different pHs of PBS at the applied potential of −0.3 V. The current increases with the increasing of the pH from 3.0 to 6.0; however, the amperometric response decreases when the pH is further increased from 7.0 to 9.0. At the lower pH ranges, the current response is very low, which might be due to the denaturation of the biomolecules (Kafi et al., 2008). Moreover, at low pH values the adsorbed Hb is positively charged and the saturation adsorption capacity decreases due to gradually increasing columbic repulsive forces between the positively charged protein amide acids. Consequently, the protein molecules require more electrode surface space, resulting in a decrease in peak current with decreasing pH. However, in pH higher than 6, the adsorbed protein molecules are negatively charged, thus the electrostatic repulsion between the protein molecules on the electrode surface can decrease the saturation adsorption capacity of Hb (Wang et al., 2005). Since the maximum amperometric response is achieved at pH 6.0, we chose the PBS buffer solution with a pH value of 6.0 as the optimized pH.

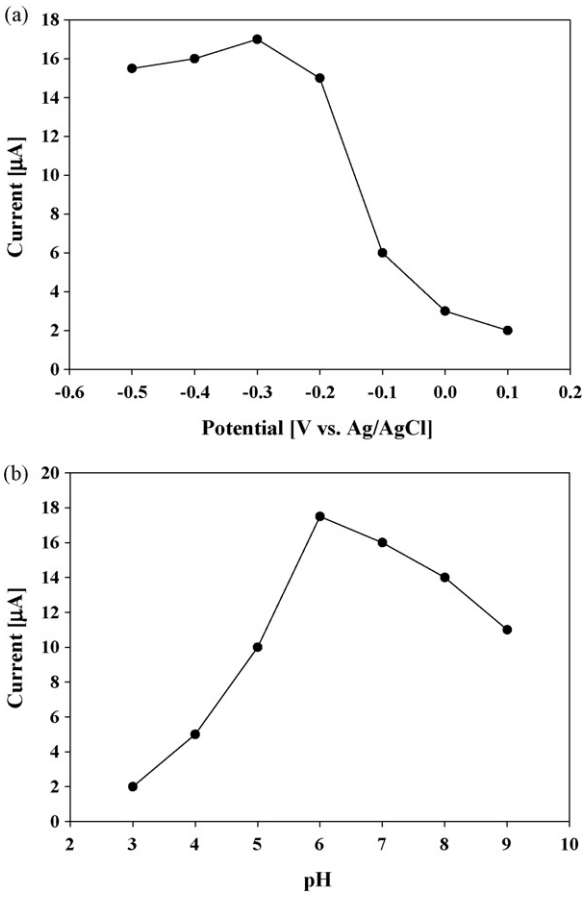

Fig. 4. (a) Dependence of current responses of the biosensor at different applied potentials measured in 0.1 M pH 7.0 PBS containing 2.5×10^{-5} mol /L H_2O_2 and (b) effect of pH on the catalytic current of the biosensor in the presence of 2.5×10^{-5} mol /L H_2O_2 in PBS at the potential of −0.3 V.

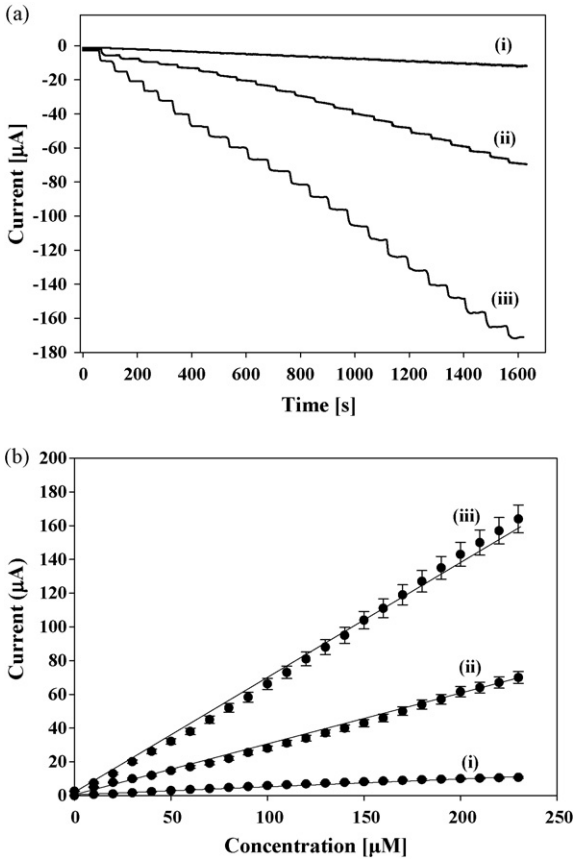

Fig. 5. (a) Steady-state amperometric response of the Ti/Hb electrode (i), the Ti/Au/Hb electrode (ii) and the Ti/NP–Au/Hb electrode (iii) with the successive additions of 1×10^{-5} M H_2O_2 in 0.1 M PBS (pH 6.0) at the operating potential of −0.3 V. (b) Calibration plots for the Ti/Hb electrode (i), the Ti/Au/Hb electrode (ii) and the Ti/NP–Au/Hb electrode (iii) with the same experimental conditions as in (a).

3.5. Amperometric response and calibration of the biosensor

The response of the biosensor was examined by testing the Ti/NP–Au/Hb electrode with H_2O_2 in increasing concentrations. The amperometric experiment was carried out in a stirred cell containing 0.1 M PBS (pH 6.0) under the optimized operating electrode potential of −0.3 V. The cathodic current responses of the (i) Ti/Hb, (ii)Ti/Au/Hb, and (iii) Ti/NP–Au/Hb electrode to H_2O_2 for each successive addition of 1×10^{-5} M are presented in Fig. 5a. A well-defined reduction current proportional to the concentration of H_2O_2 is observed at the Ti/NP–Au/Hb electrode. The reaction occurring at the Ti/NP–Au/Hb electrode (Plot iii) very quickly reaches a dynamic equilibrium upon each addition of the sample solution, generating a steady-state current signal within 5–10 s. However, much lower current responses are found both at the Ti/Hb and Ti/Au/Hb electrodes. Fig. 5b shows the typical calibration curves of the (i) Ti/Hb, (ii) Ti/Au/Hb, and (iii) Ti/NP–Au/Hb electrode. The calibration plot of the Ti/NP–Au/Hb electrode for H_2O_2 detection shows a linear response up to 2.5×10^{-4} M H_2O_2 with a correlation coefficient of 0.997. The detection limit was determined to be 2×10^{-8} M (based on S/N = 3).

The Michaelis–Menten constant (K_m) gives information regarding the enzyme–substrate kinetics (Shu and Wilson, 1976). According to the Michaelis–Menten equation:

$$\frac{I_{max}}{I_s} = \frac{K_m}{C + 1}$$

where I is the steady-state catalytic current, I_{max} is the maximum current measured under saturated conditions, C refers to the concentration of H_2O_2 and K_m stands for the apparent Michaelis–Menten constant. The K_m was estimated to be 0.261 mM for Ti/NP–Au/Hb; the small K_m value indicates that the immobilized Hb on the nanoporous Au networks possesses high enzymatic-like activity for H_2O_2 reduction.

Table 1
Comparison of the performances of the various types of H_2O_2 biosensors.

Modified electrode	Linear range (M)	Detection limit (μM)	Stability	Reference
HRP/Au	1.0×10^{-4} to 3.9×10^{-3}	2.0	96% (30 days)	Camacho et al. (2008)
HRP/Au/TiO_2 nanotube	5.0×10^{-6} to 4.0×10^{-4}	2.0	95% (45 days)	Kafi et al. (2008)
HRP/Carbon NT/MB	4.0×10^{-6} to 2.0×10^{-3}	1.0	80% (2 weeks)	Xu et al. (2003)
Hb in TiO_2 nanotube	4.0×10^{-6} to 6.4×10^{-5}	4.6	90% (21 days)	Zheng et al. (2008a,b)
Hb in polymer/Au	1.0×10^{-5} to 45×10^{-4}	0.5	82% (21 days)	Mingrui et al. (2006)
NPG/GCE	2.0×10^{-4} to 2.5×10^{-3}	ND	ND	Qiu et al. (2009)
Hb/Ti/nano-Au network	5.0×10^{-8} to 2.0×10^{-4}	0.02	95% (45 days)	This work

Hb, hemoglobin; HRP, horseradish peroxide; NT, nanotube; MB, methylene blue; NPG, nanoporous gold; GCE, glassy carbon electrode.

3.6. Stability and reproducibility of the biosensor

The stability of the biosensor was studied over a period of 45 days with storage of the Ti/NP–Au/Hb electrode in a PBS buffer solution with the pH value of 7.0 at 4 °C. The biosensor retained 95% of its initial sensitivity after 45 days of operation. The repeatability of a Ti/NP–Au/Hb electrode was tested in the presence of 0.25 mM of H_2O_2 in 0.1 M PBS (pH 6.0). The repeatability of the biosensor was calculated by five repetitive experiments on the same day under the optimal working conditions. The relative standard deviation was 3.2% for the five successive assays and 5.1% for 3 electrodes fabricated in the same manner for the H_2O_2 amperometric detection. The response of the fabricated Ti/NP–Au/Hb electrode to the common interfering species ascorbic acid and uric acid (which usually coexist in samples) was also evaluated under the optimized experimental condition (−0.3 V), showing that there was no response to 0.1 mM ascorbic acid and 0.1 mM uric acid. The performance of the Ti/NP–Au/Hb biosensor developed in this study was compared with other biosensors as listed in Table 1. This reveals that our proposed biosensor shows excellent performance in terms of low detection limit, long linear range and high stability.

4. Conclusions

In conclusion, nanoporous Au networks were directly grown onto a Ti substrate by chemical reduction of an Au precursor under a hydrothermal condition. Direct electrochemistry of Hb immobilized on the nanoporous Au network was observed. The fabricated Ti/NP–Au/Hb biosensor effectively sensed successive increases of H_2O_2 with long linear range, low detection and short response time. The biosensor shows very high sensitivity, good reproducibility and long-time stability. Under the optimized conditions, the linearity of the developed biosensor for the detection of H_2O_2 spans from 5×10^{-8} to 2×10^{-4} M with a detection limit of 2×10^{-8} M (based on S/N = 3). The promising results presented in this study show that the nanoporous Au networks are an excellent matrix for enzyme immobilization, opening a new door for the development of high-performance electrochemical biosensors.

Acknowledgments

This work was supported by a Discovery Grant from the Natural Sciences and Engineering Research Council of Canada (NSERC). A.K.M. Kafi acknowledges the Ontario Post Doctoral Fellowship. A. Chen acknowledges NSERC and the Canada Foundation of Innovation (CFI) for the Canada Research Chair Award in Material and Environmental Chemistry.

References

Ahmadalinezhad, A., Kafi, A.K.M., Chen, A., 2009. Electrochem. Commun. 11, 2048–2051.
Batchelor-McAuley, C., Wildgoose, G.G., Compton, R.G., 2009. Biosens. Bioelectron. 24, 3183–3190.
Beissenhirtz, M.K., Elnathan, R., Weizmann, Y., Willner, I., 2007. Small 3, 375–379.
Benvenuto, P., Kafi, A.K.M., Chen, A., 2009. J. Electroanal. Chem. 627, 76–81.
Camacho, C., Matias, J.C., Cao, R., Matos, M., Chico, B., Hernandez, J., Longo, M.A., Sanroman, M.A., Villalonga, R., 2008. Langmuir 24, 7654–7657.
Chen, H.J., Dong, S.J., 2007. Biosens. Bioelectron. 22, 1811–1815.
Duan, G., Li, Y., Wen, Y., Ma, X., Wang, Y., Ji, J., Wu, P., Zhang, Z., Yang, H., 2008. Electroanalysis 20, 2454–2459.
Erlebacher, J., Aziz, M.J., Karma, A., Dimitrov, N., Sieradzki, K., 2001. Nature 410, 450–453.
Feng, J.-J., Xu, J.-J., Chen, H.-Y., 2005. J. Electroanal. Chem. 585, 44–50.
Gao, L., Gao, Q., 2007. Biosens. Bioelectron. 22, 1454–1460.
Gooding, J.J., 2006. Small 2, 313–315.
Highton, L., Kadara, R.O., Jenkinson, N., Riehl, B.L., Craig, E., Banks, C.E., 2009. Electroanalysis 21, 2387–2389.
Holt-Hindle, H., Nigro, S., Asmussen, M., Chen, A., 2008. Electrochem. Commun. 10, 1438–1441.
Huang, J.F., Sun, I.W., 2005. Adv. Funct. Mater. 15, 989–994.
Kafi, A.K.M., Chen, A., 2009. Talanta 79, 97–102.
Kafi, A.K.M., Wu, G., Chen, A., 2008. Biosens. Bioelectron. 24, 566–571.
Katz, E., Willner, I., 2004. Angew. Chem. Int. Ed. 43, 6042–6108.
Khan, R., Dhayal, M., 2008. Electrochem. Commun. 10–2, 263–267.
Kissinger, P.T., 2005. Biosens. Bioelectron. 15, 2512–2516.
Kongcheng, H., Dongxiao, L., Xuemei, L., Shusheng, Z., 2008. Anal. Chem. 80, 9124–9130.
Koczkur, K., Yi, Q.F., Chen, A., 2007. Adv. Mater. 19, 2648–2652.
Kumar, C.V., Chaudhari, A., 2002. Chem. Commun., 2382–2383.
Li, M., Deng, C., Chen, C., Peng, L., Ning, G., Xie, Q., Yao, S., 2006. Electroanalysis 18, 2210–2217.
Lim, I.S., Mott, D., Ip, W., Njoki, P.N., Pan, Y., Zhou, S., Zhong, C.J., 2008. Langmuir 24, 8857–8863.
Liu, S., Bakovic, L., Chen, A., 2006. J. Electroanal. Chem. 591, 210–216.
Liu, S., Chen, A., 2005. Langmuir 21, 8409–8413.
Luong, J.H., Male, K.B., Glennon, J.D., 2008. Biotechnol. Adv. 26, 492–500.
Matthew, C.D., Thomas, A.D., Mitsunori, H., Smilgies, D.F., Moses, H.W.C., David, L.A., 2007. Langmuir 23, 2414–2422.
Mehrvar, M., Abdi, M., 2004. Anal. Sci. 20, 1113–1126.
Michel, M., Taylor, A., Sekol, R., Podsiadlo, P., Ho, P., Kotov, N., Thompson, L., 2007. Adv. Mater. 19, 3859–3864.
Mingrui, L., Chunyan, D., Chao, C., Limei, P., Guohong, N., Qingji, X., Shouzhuo, Y., 2006. Electroanalysis 18, 2210–2217.
Moulder, J.F., Stickle, W.F., Sobol, P.E., Bomben, K.D., 1995. Handbook of X-ray Photoelectron Spectroscopy. Physical Electronics, Inc., Eden Prairie, MN.
Murray, R.W., 1984. Electroanal. Chem. 13, 191–368.
Qiu, H., Xue, L., Ji, G., Zhou, G., Huang, X., Qu, Y., Gao, P., 2009. Biosens. Bioelectron. 24, 3014–3018.
Shulga, O.V., Zhou, D., Demchenko, A.V., Stine, K.J., 2008. Analyst 133, 319–322.
Shu, F.R., Wilson, G.S., 1976. Anal. Chem. 48, 1679–11679.
Tian, M., Kanavillil, N., Davey, L., Leung, K.T., Schraft, H., Chen, A., 2007. J. Electroanal. Chem. 611, 133–139.
Wanekaya, A.K., Chen, W., Mulchandani, A., 2008. J. Environ. Monit. 10, 703–712.
Wang, C.H., Yang, C., Song, Y.Y., Gao, W., Xia, X.H., 2005. Adv. Funct. Mater. 15, 1267–1275.
Wang, J., 2008. Chem. Rev. 108, 814–825.
Wang, J., Musameh, M., Lin, Y., 2003. J. Am. Chem. Soc. 125, 2408–2409.
Wang, J., Thomas, D.F., Chen, A., 2008. Chem. Commun., 5010–5012.
Wang, L., Wang, E., 2004. Electrochem. Commun. 6, 225–229.
Wang, Y., Chen, X., Zhu, J.J., 2009. Electrochem. Commun. 11, 323–326.
Xu, C., Su, J., Xu, X., Liu, P., Zhao, H., Tian, F., Ding, Y., 2007. J. Am. Chem. Soc. 129, 42–43.
Xu, J.Z., Zhu, J.J., Wu, Q., Hu, Z., Chen, H.Y., 2003. Electroanalysis 15, 219–224.
Yan, Y., Zheng, W., Zhang, M., Wang, L., Lei, S., Mao, L., 2005. Langmuir 21, 6560–6566.
Yang, H., Fung, S.Y., Pritzker, M., Chen, P., 2009. Langmuir 25, 7773–7777.
Zeis, R., Mathru, A., Fritz, G., Lee, J., Erlebacher, J., 2007. J. Power Sources 165, 65–72.
Zhang, J.T., Liu, P.P., Ma, H.Y., Ding, Y., 2007. J. Phys. Chem. C 111, 10382–10388.
Zheng, W., Li, J., Zheng, Y.F., 2008a. Biosens. Bioelectron. 23, 1562–1566.
Zheng, W., Zheng, Y.F., Jin, K.W., Wang, N., 2008b. Talanta 74, 1414–1419.
Zhu, A.W., Tian, Y., Liu, H.Q., Luo, Y.P., 2009. Biomaterials 30, 3183–3188.